



Weakening of the subduction interface and its effects on surface heat flow, slab dehydration, and mantle wedge serpentinization

Ikuko Wada,¹ Kelin Wang,^{1,2} Jiangheng He,² and Roy D. Hyndman^{1,2}

Received 29 May 2007; revised 18 October 2007; accepted 7 December 2007; published 2 April 2008.

[1] The shallow part of the interface between the subducting slab and the overriding mantle wedge is evidently weakened by the presence of hydrous minerals and high fluid pressure. We use a two-dimensional finite element model, with a thin layer of uniform viscosity along the slab surface to represent the strength of the interface and a dislocation-creep rheology for the mantle wedge, to investigate the effect of this interface “decoupling.” Decoupling occurs when the temperature-dependent viscous strength of the mantle wedge is greater than that of the interface layer. We find that the maximum depth of decoupling is the key to most primary thermal and petrological processes in subduction zone forearcs. The forearc mantle wedge above a weakened subduction interface always becomes stagnant (<0.2% slab velocity), providing a stable thermal environment for the formation of serpentinite. The degree of mantle wedge serpentinization depends on the availability of aqueous fluids from slab dehydration. A very young and warm slab releases most of its bound H₂O in the forearc, leading to a high degree of mantle wedge serpentinization. A very old and cold slab retains most of its H₂O until farther landward, leading to a lower degree of serpentinization. Our preferred model for northern Cascadia has a maximum decoupling depth of about 70–80 km, which provides a good fit to surface heat flow data, predicts conditions for a high degree of serpentinization of the forearc mantle wedge, and is consistent with the observed shallow intraslab seismicity and low volume of arc volcanism.

Citation: Wada, I., K. Wang, J. He, and R. D. Hyndman (2008), Weakening of the subduction interface and its effects on surface heat flow, slab dehydration, and mantle wedge serpentinization, *J. Geophys. Res.*, *113*, B04402, doi:10.1029/2007JB005190.

1. Introduction

[2] The thermal structure of a subduction zone is the primary control of its earthquake and volcanic processes [e.g., Kirby *et al.*, 1996]. The thermal state is strongly controlled by solid-state viscous flow in the wedge-shaped mantle region between the subducting and overriding plates. Beneath the volcanic arc, the wedge flow is inferred to be driven primarily by the downgoing slab and has been modeled as basally driven corner flow [Batchelor, 1967]. The flow brings in hot material from greater depths to replace cold material that travels down dip with the slab (Figure 1a). This circulation is responsible for the ongoing high temperature required for arc magmatism. However, geophysical and geological evidence indicates that most of the forearc mantle wedge does not participate in this flow.

[3] The most direct evidence is surface heat flow. Heat flow decreases arcward from the trench to values as low as 30–40 mW/m² before it increases to the arc and back arc values of ~80 mW/m² (Figure 1b) [Currie and Hyndman,

2006]. The initial decrease is the direct cooling effect of the subducting slab, and the eventual landward increase is due to advective heat transport by mantle wedge flow. Without the wedge flow, surface heat flow would continue to decrease landward (Figure 1b). Where the heat flow begins to increase depends on the seaward limit of mantle wedge flow. The pattern of observed heat flow indicates that thermally significant wedge flow does not begin until near the volcanic arc. In order to fit heat flow observations, a number of authors have concluded that a trenchward part of the mantle wedge beneath the forearc must be stagnant [Furukawa and Uyeda, 1989; Furukawa, 1993; Peacock and Wang, 1999; van Keken *et al.*, 2002; Currie *et al.*, 2004a].

[4] Another line of evidence for a stagnant forearc mantle wedge is the presence of hydrous minerals in it, particularly serpentine that is stable only at relatively low temperatures (Figure 1a). Mantle wedge serpentinization has been inferred from geological evidence such as serpentine mud volcanoes and from geophysical observations such as lower seismic wave speeds and high Poisson’s ratio in the forearc mantle wedge [Hyndman and Peacock, 2003, and references therein]. For example, low seismic wave speeds observed in the Cascadia forearc mantle, resulting in a diminished or inverted seismic velocity contrast across the continental Moho, have been interpreted as to indicate serpentinization [Bostock *et al.*, 2002; Brocher *et al.*,

¹School of Earth and Ocean Sciences, University of Victoria, Victoria, British Columbia, Canada.

²Pacific Geoscience Centre, Geological Survey of Canada, Sidney, British Columbia, Canada.

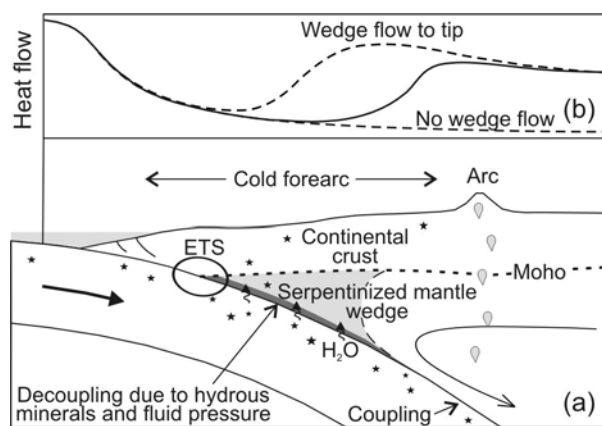


Figure 1. Schematic illustration of a typical warm-slab subduction zone and its surface heat flow. (a) Forearc mantle wedge and its environment. Stars represent intraplate earthquakes. ETS is episodic slip and tremor observed at Cascadia and Nankai, to be discussed in section 5.1. ETS may be rare in cold-slab subduction zones. (b) Surface heat flow (solid curve). Heat flow patterns for cold-slab subduction zones are similar, except that values near the trench and further seaward are much lower. Models that do not include mantle wedge flow or allow the flow to occur near the tip of the wedge would incorrectly predict the heat flow pattern (dashed curves).

2003]. This interpretation is supported by results of seismic tomography [Ramachandran *et al.*, 2005] and positive magnetic anomalies and negative gravity anomalies in the Cascadia forearc [Blakely *et al.*, 2005]. Serpentinization of the forearc mantle wedge has also been proposed for southwest Japan [Kamiya and Kobayashi, 2000; Seno *et al.*, 2001], central Andes [Graeber and Asch, 1999], and Costa Rica [DeShon and Schwartz, 2004]. The serpentinization suggests conditions of relatively low temperatures and high contents of aqueous fluids [Hyndman and Peacock, 2003]. Such conditions cannot be sustained if there is vigorous mantle wedge flow because the flow would continuously replenish the forearc mantle wedge with dryer and hotter material brought up from greater depths.

[5] A number of studies show seismic attenuation in the forearc mantle wedge to be low, which is in sharp contrast with high attenuation in the subarc mantle and is thought to indicate low temperatures in a stagnant forearc mantle wedge [e.g., Tsumura *et al.*, 2000; Wiens and Smith, 2003; Stachnik *et al.*, 2004; Abers *et al.*, 2006]. Well-located earthquakes in the forearc mantle wedge [e.g., Hasegawa *et al.*, 1994; Nakajima *et al.*, 2001; Miura *et al.*, 2003], although rare, also indicate low temperatures that are required for seismic failure.

[6] The necessary condition for the forearc mantle wedge to become stagnant is that its basal drag force is very small relative to the strength of the overlying material, that is, the slab and the mantle wedge must be adequately decoupled [Furukawa, 1993]. As explained by Peacock and Hyndman [1999] and will be further discussed in the following section, the presence of hydrous minerals, such as serpentine and talc, and high fluid pressure will surely weaken the subduction interface and cause decoupling. With decou-

pling, a feedback mechanism can be qualitatively established as follows.

[7] The cooling effect of the subducting slab results in relatively low temperatures in the most seaward part of the mantle wedge. Fluids released from the subducting slab during metamorphic dehydration will allow weak hydrous minerals to form and will elevate pore fluid pressure along the slab-mantle wedge interface. Solid-state mantle wedge flow directly above the weakened interface will thus be slow or absent. Stagnation of the mantle wedge in turn feeds back to help maintain a cool and wet condition to facilitate the formation of hydrous minerals, maintaining or enhancing interface decoupling. In this process, serpentinization of the forearc mantle wedge begins from its base but, with sufficient and lasting fluid supply from the slab, the entire stagnant portion may be highly serpentinized, especially at its tip. Serpentinization decreases rock density [Christensen, 1996], and the resultant buoyancy works against slab-driven downward flow, further stabilizing the forearc mantle wedge.

[8] In this study, we use numerical modeling to study a key aspect of this complex process, namely, how the weakening of the subduction interface affects the dynamics of wedge flow and the thermal and petrological states of the forearc mantle wedge and subducting slab. Our models are generic, steady-state, and two-dimensional. In our models, the strength of the subduction interface is prescribed. Metamorphic reactions and water flow are not included except as the proposed mechanism for altering interface properties. The complex, nonlinear feedbacks between thermal, hydrological, mineralogical, and mechanical processes are only qualitatively discussed. These simplifications are technically necessary given the lack of constraints on many parameters involved. They are also intellectually important, because it is focused studies of key processes that bring about physical insights. We apply the model to northern Cascadia, an end-member warm-slab subduction zone for which ample geophysical observations are available, but we also test the effects of cold-slab subduction.

[9] In the following sections, we first briefly review mechanisms that cause weakening of the subduction interface. We then describe the model setup, including how the weakened subduction interface is represented in the modeling. When presenting model results, we demonstrate how the thermal and petrological regimes are affected by various degrees of decoupling. The implications of the model results for intraslab earthquakes, arc volcanism, and mantle wedge anisotropy are discussed in section 5.

2. Weakening of the Slab-Mantle Wedge Interface in the Forearc

[10] Hydration of olivine, the most abundant mineral in dry mantle peridotite, produces serpentine minerals. Of the three serpentine species (chrysotile, lizardite, and antigorite), only antigorite is stable at temperatures above 250°C [Evans, 1977], and it is expected to be the most abundant hydrous mineral in a hydrated continental forearc mantle wedge [Hyndman and Peacock, 2003]. At ocean-ocean convergent margins, the shallow part of the forearc mantle wedge is at much lower temperatures because of the very thin overriding crust, and the other two serpentine species

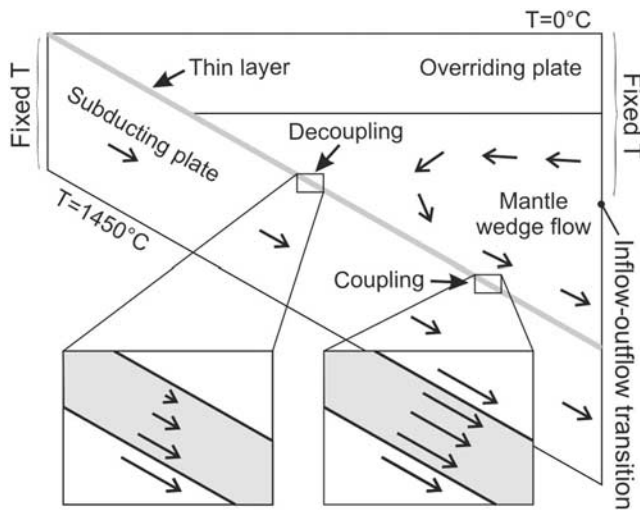


Figure 2. Schematic illustration of boundary and interface conditions for the thermal models. Insets show how the velocity varies across the thin layer along the interface in the cases of decoupling and coupling.

can be stable [Evans, 1977, 2004]. Chlorite forms through hydration of orthopyroxene, the second most abundant mineral in dry peridotite [Goto and Tatsumi, 1990]. Antigorite and chlorite contain 12.3 and 13 wt% H₂O, respectively, and dominate the fluid budget of the forearc mantle [Schmidt and Poli, 1998]. Other hydrous minerals in H₂O-saturated mantle peridotite at pressures and temperatures appropriate for the forearc mantle wedge include brucite and amphibole. Fluids released from the subducting slab are likely to be silica-saturated. Addition of these fluids to silica-undersaturated mantle wedge material produces talc in addition to the above primary hydrous minerals [Peacock and Hyndman, 1999].

[11] Because the fluid source in the subduction zone is the dehydrating slab, the wettest part of the forearc mantle wedge should be its base. Therefore, hydrous minerals are likely to be most abundant along and just above the subduction interface. Hydrous minerals are generally weaker than anhydrous minerals that would be found in a dry mantle wedge [e.g., Morrow et al., 2000; Christensen, 2004] and can substantially weaken the subduction interface.

[12] From the continental Moho down to ~70 km depth, talc is expected to be abundant along the interface and may be a dominant agent of weakening [Peacock and Hyndman, 1999]. Its abundance along the interface is supported by field observations of talc-rich serpentinites that are inferred to have been derived from the slab-mantle wedge interface [e.g., Peacock, 1987; Bebout and Barton, 1989]. Although the dynamic frictional behavior of talc in terms of seismogenic stick-slip versus aseismic stable-sliding is yet to be experimentally investigated, its general weakness is widely recognized. As a fault gouge, its coefficient of friction under wet conditions is as low as ~0.2 [Morrow et al., 2000]. Other hydrous minerals may also contribute to interface weakening. For example, the friction coefficients of brucite, chlorite, and antigorite-rich gouge are reported to be ~0.3, ~0.4, and ~0.5, respectively [Morrow et al., 2000]. The sheeted structure of these phyllosilicate minerals and loose

bonding of water to the mineral surface both lead to low frictional strength.

[13] Elevated pore fluid pressure further reduces the frictional strength of the interface. For example, if the pore fluid pressure is 90% of lithostatic pressure, the effective friction coefficient will be lower than the intrinsic friction coefficient by an order of magnitude. Although still difficult to constrain with direct measurements, pore fluid pressure along the interface is expected to be high and probably decreases upward into the mantle wedge. It has been argued that upward migration of aqueous fluids from the dehydrating slab is possible only through permeability creation via hydrofracturing [Peacock and Hyndman, 1999]. Hydrofracturing requires pore fluid pressure to exceed the minimum principal stress, and the most likely place to reach this state is the base of the mantle wedge which is nearest to the fluid source.

[14] It is important to recognize that decoupling or coupling depends also on the strength of the overlying mantle material. If the mantle wedge deforms as readily as does the interface, there will be no decoupling. Because of an extremely high sensitivity to temperature, the mantle material is strong at shallow depths where the temperature is low and becomes very weak at greater depths where the temperature is high. Thus, the weakening of the mantle wedge with increasing depth diminishes the strength contrast between the interface and mantle wedge, eventually resulting in full coupling. Beneath the volcanic arc, the presence of melts further reduces the viscous strength of the mantle material.

3. Model Description

3.1. Material Properties, Geometry, and Boundary Conditions

[15] We use a steady state two-dimensional finite element model with prescribed slab motion. The model consists of a rigid overriding plate, a rigid subducting slab, and a viscous mantle wedge (Figure 2). The governing equations for the flow and temperature fields are as shown in the work of van Keken et al. [2002] except for the addition of viscous energy dissipation, and the numerical method is exactly as described in the work of Currie et al. [2004a].

[16] For the mantle wedge, we invoke the dislocation-creep rheology. Using the customary uniaxial-deformation expression, the relation between axial strain rate ($\dot{\epsilon}_a$) and stress (σ_a) for dislocation creep is [Karato and Wu, 1993]

$$\dot{\epsilon}_a = A \left(\frac{\sigma_a}{\mu} \right)^n \exp \left(-\frac{E}{RT} \right) \quad (1)$$

where A and n are constants, μ is shear modulus (80 GPa in this study), E is activation energy, R is the universal gas constant (8.3145 J mol⁻¹ K⁻¹), and T is absolute temperature. There is a pressure term in the original version of (1), but its effect is very small and is neglected here. A number of experimentally constrained rheological parameter values for olivine aggregates are available, including those that account for the effects of melts and aqueous fluids [e.g., Hirth and Kohlstedt, 2003]. However, for the purpose of this study, we are interested only in the overall nonlinear behavior of dislocation creep, and the specific choice of

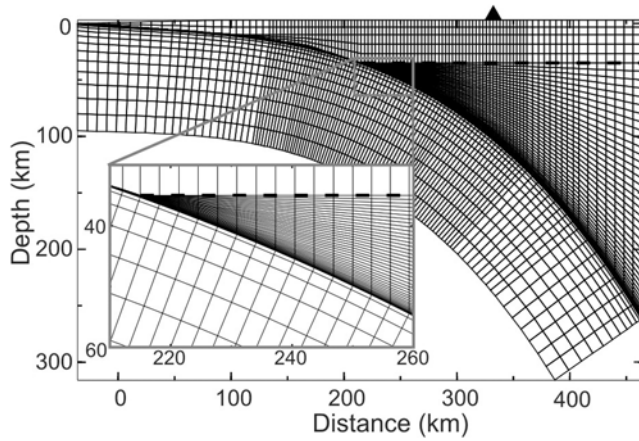


Figure 3. A typical finite element mesh used in this work. The triangle on top represents the average location of the volcanic arc at northern Cascadia. The mesh used for a model of fully coupled interface has a much finer mesh in the mantle wedge corner than shown here.

parameter sets is unimportant. For the models to be discussed in section 4, we take the widely cited parameter values of $A = 2 \times 10^{18} \text{ s}^{-1}$, $n = 3$, and $E = 430 \text{ kJ/mol}$ reported by *Karato and Wu* [1993] for wet olivine. In our modeling, expression (1) is cast into the relation between deviatoric strain rate ($\dot{\epsilon}_{ij}$) and deviatoric stress (σ_{ij}) $\sigma_{ij} = 2\eta_e \dot{\epsilon}_{ij}$, where

$$\eta_e = 3^{-\frac{(n+1)}{2}} \frac{\mu}{A} \left(\frac{\mu}{\sigma}\right)^{n-1} \exp\left(\frac{E}{RT}\right) \quad (2)$$

is the effective viscosity, with σ being the second invariant of σ_{ij} [Ranalli, 1995]. For two-dimensional flow of an incompressible fluid ($\dot{\epsilon}_{33} = 0$), because σ_{33} is unknown without knowing η_e a priori, σ has to be calculated from $\dot{\epsilon}$, the second invariant of $\dot{\epsilon}_{ij}$, assuming $\dot{\epsilon} = 3^{\frac{n+1}{2}} \frac{A}{2} \left(\frac{\sigma}{\mu}\right)^n \exp\left(-\frac{E}{RT}\right)$ [Ranalli, 1995]. Note that

the η_e expression in the work of *Ranalli* [1995] differs from (2) by a factor of two because he used the engineering definition of strain rate. Other methods have also been used to cast (1) into a form suitable for two- and three-dimensional modeling [e.g., *Chen and Morgan*, 1990; *van Keken et al.*, 2002]. The differences between different methods are overshadowed by uncertainties in extrapolating laboratory results that were used to derive (1) to in situ conditions and in the effects of H_2O and melt contents on η_e .

[17] Our model differs from that of *Currie et al.* [2004a] by including frictional heating and viscous energy dissipation. Frictional heating Q_{FH} along the subduction interface is the product of fault slip rate and shear stress $\tau = \mu' \sigma_n$, where σ_n is normal stress and μ' is the effective coefficient of friction. We use the weight of the overriding rock column to approximate σ_n and assume $\mu' = 0.03$ which is consistent with the concluded low strength of the Cascadia subduction fault [Wang et al., 1995] and other large active faults. Viscous heating Q_{VD} along the ductile part of the subduc-

tion interface and in the mantle wedge is calculated from the product of shear stress and shear strain rate.

[18] We use a finite element mesh consisting of about 7200 elements of variable sizes (dimensions ranging from $\sim 1 \text{ m}$ to $\sim 10 \text{ km}$). For temperatures, velocities, and coordinates, each element has nine nodal points. For pressure, only the four corner nodes of each element are used. The total number of temperature nodal points is about 29,300. Details of the mesh vary between different test cases to allow optimal distributions of element density. A typical mesh used in this study is shown in Figure 3. Our slab geometry is a regional average for northern Cascadia and is similar to, although smoother than, that of *Currie et al.* [2004a]. We use a constant model grid thickness of 95 km for the subducting plate, but the thermally relevant “slab thickness” is actually defined by the temperature profile assigned to the plate at the trench-side vertical boundary [Peacock and Wang, 1999]. We assign zero velocities to nodes in the top 35 km of the overriding plate, but the actual base of the “rigid” upper plate is deeper, at a thermally controlled rheological transition determined as part of the solution. We use a subduction velocity of 4.5 cm/a, appropriate for northern Cascadia. At the vertical boundary on the back-arc side, material is allowed to flow in across the shallow part of this boundary and out across its deep part. The depth of inflow to outflow transition is determined iteratively within the modeling code.

[19] We assign constant temperatures of 0°C and 1450°C to the upper and the lower boundaries of the model, respectively. To model the warm-slab subduction at northern Cascadia, we apply a geotherm calculated for a cooling oceanic plate of 8 Ma in age [Stein and Stein, 1992] to the trench-side vertical boundary. The age-controlled thermal structure of the incoming plate has a first-order influence on the thermal state of the subduction zone [e.g., *Peacock and Wang*, 1999]. To investigate the effects of a cold slab, we also run models for a 130-Ma-old incoming plate. Following *Currie et al.* [2004a], we use a back-arc geotherm for the back-arc-side vertical boundary from the surface to 60 km depth. Between this depth and the depth of the inflow-outflow transition, we assign a geotherm calculated using an adiabatic gradient of 0.3°C/km and a mantle potential temperature of 1295°C [Ito and Katsura, 1989]. The one-dimensional continental geotherm with an upper-crust heat generation of $1.3 \mu\text{W/m}^3$ gives a surface heat flow of 75 mW/m^2 , similar to typical back arc heat flow values of $\sim 80 \text{ mW/m}^2$ [Currie and Hyndman, 2006] and to the average value in the Cascadia back arc [Lewis et al., 1992]. The thermal parameters used in this study are summarized in Table 1.

[20] Although an adiabatic thermal gradient is applied at the vertical boundary below 60 km depth, the effect of

Table 1. Thermal Properties Used in the Finite Element Models

Property	Material	Value
Thermal conductivity (W/mK)	Continental crust	2.5
	Mantle wedge	3.1
	Slab	3.1
Heat generation ($\mu\text{W/m}^3$)	Upper crust (15-km-thick)	0.2–1.3
	Lower crust (20-km-thick)	0.4
	Mantle	0.02
	Slab	0.02

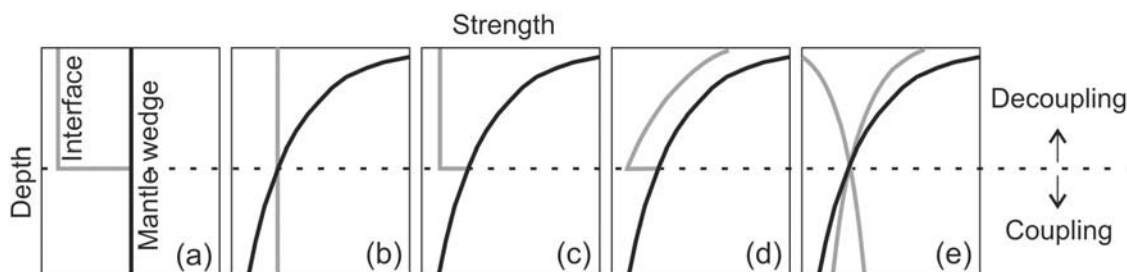


Figure 4. Different idealized forms of downdip decoupling termination. (a) Uniform interface strength and isoviscous mantle wedge. An increase in interface strength terminates decoupling. (b) Uniform interface strength but temperature-dependent mantle wedge rheology. The termination of decoupling is thermally controlled. (c) A hybrid of Figures 4a and 4b. (d) Similar to Figure 4c, but the interface has the same rheology as but is weaker than the mantle wedge. (e) Other combinations of interface and mantle strength profiles.

adiabatic heating due to mantle flow is neglected because of the assumption of incompressible flow. *Currie* [2004] conducted numerical tests and showed this effect to be small at depths less than 200 km. Also commonly neglected by models of this type are volume changes due to metamorphic phase changes.

[21] As *Currie et al.* [2004a] have shown, if the back-arc-side boundary is placed far away from the arc, the model based on the temperature- and stress-dependent rheology predicts back-arc heat flows that are significantly lower than observed. To maintain high heat flow in the back arc, some heat transport mechanisms other than slab-driven flow are needed. *Currie et al.* [2004a] suggested that vigorous small-scale convection (buoyancy-driven flow) in the back arc mantle probably causes the observed high heat flow. In the forearc, buoyancy-driven flow is discouraged because of the narrow space and relatively small temperature difference between the top and bottom of the mantle wedge. The transition between buoyancy-driven and slab-driven flow regimes must take place somewhere in the arc and back arc region. Because we focus on the forearc region, we put the back-arc-side boundary at a short distance (130 km) landward of the arc and only simulate slab-driven flow.

3.2. Interface Coupling and Decoupling

[22] Various methods have been used to simulate slab-mantle decoupling in previous model studies. In the work of *Currie et al.* [2004a], and also in the work of *Peacock and Wang* [1999] and *van Keken et al.* [2002], a no-flow condition was imposed on the most seaward part of the mantle wedge. This “rigid corner” prevented mantle wedge flow from entering this region, resulting in a surface heat flow pattern consistent with that observed. *Conder* [2005] used an improved version of this approach in which the size and shape of the rigid corner are defined by a thermally controlled brittle-ductile transition. *Kneller et al.* [2005, 2007] and *Abers et al.* [2006] used a kinematically prescribed velocity discontinuity across the interface. Full coupling or complete decoupling is accomplished by allowing the mantle material just above the interface to move at the slab velocity or be fixed, respectively, and any intermediate differential velocity represents partial decoupling. *Furukawa* [1993] used a free slip (i.e., zero shear stress) condition to simulate decoupling, so that there is no need to prescribe a differential velocity across the interface.

[23] In our model, we use a thin layer of low viscosity along the interface, in effect simulating a stress condition (Figure 2). This thin layer does not need to represent a specific component of the subduction system. It represents the collective effect of various mechanisms that weaken the interface discussed in section 2. If the thin layer is less viscous than the overriding mantle, shear strain is localized within it, resulting in a sharp but continuous decrease in flow velocity across the layer (Figure 2). This is one step forward from the free-slip approach of *Furukawa* [1993] because it can accommodate a range of stress conditions from complete decoupling to full coupling. Complete decoupling, that is, the velocity decreases to zero across the layer, occurs when the layer is very weak. Full coupling occurs when the layer is as strong as or stronger than the overriding mantle.

[24] We use a uniform viscosity (η') for the thin layer to represent the strength of the subduction interface. This choice of layer rheology is arbitrary, but given the present state of knowledge of the actual processes along the interface, we do not deem more complex parameterizations useful for the purpose of the present study. A simplifying feature of an isoviscous layer is that its strength scales with the ratio of its viscosity and thickness. Because of this scaling relationship, the absolute value of the layer thickness or viscosity is unimportant. We choose to vary the degree of decoupling by changing the layer viscosity using a fixed layer thickness of 100 m, for which the model is numerically stable over a wide range of layer viscosities.

[25] The frictionally coupled part of the subduction interface where Q_{FH} is calculated is assumed to extend from the trench to a temperature of 400°C or the continental Moho, whichever is shallower. Below the continental Moho, Q_{VD} is calculated using the viscosity and strain rate of the thin layer along the interface. If the intersection of the interface with the 400°C isotherm is shallower than the Moho, a function similar to (1) is used to allow a smooth transition from the shallow Q_{FH} to the thin-layer Q_{VD} .

[26] Figure 4 shows possible forms of downdip decoupling termination as controlled by the strength contrast between the thin layer and the mantle wedge. With a hypothetical isoviscous mantle wedge (Figure 4a), the strength contrast is uniform, such that decoupling can be terminated only by limiting the downdip length of the

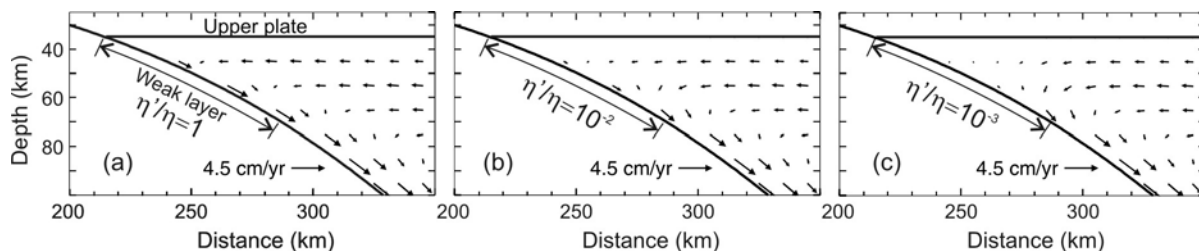


Figure 5. Flow fields calculated in a model with a mantle wedge of uniform viscosity η and an interface layer of viscosity η' that extends to 70 km depth. (a) Full coupling. (b) Partial decoupling. (c) Almost complete decoupling.

thin layer. With a more realistic temperature- and stress-dependent mantle wedge rheology, the mantle strength decreases with increasing temperature and hence depth (Figure 4b), and decoupling is terminated where the strength contrast disappears. In this case, the downdip length of the thin layer has no effect as long as it extends beyond the temperature-controlled termination depth. The scenario in Figure 4c is a hybrid of those in Figures 4a and 4b. A very weak layer can be used to simulate complete decoupling over the length of the layer extending to the prescribed maximum depth of decoupling. The free-slip decoupling model of *Furukawa* [1993] can be viewed as an end-member case of this model (zero layer viscosity). In the scenario shown in Figure 4d, the layer has the same rheology as the mantle wedge, but is much weaker. Similarly to that in Figure 4a, decoupling can be terminated only by truncating the thin layer at some depth. Figure 4e shows other possible combinations of layer and mantle wedge rheology.

[27] Here, we first use a mantle wedge of uniform viscosity η (scenario in Figure 4a) to illustrate how the thin layer defines the degree of decoupling. The results of this simple model will be useful for interpreting models with a more realistic mantle wedge rheology discussed in section 4. In this model, we let the thin layer extend to 70 km depth, the depth of the bottom of the “rigid corner” of *Currie et al.* [2004a]. The strength contrast between the layer and the isoviscous mantle wedge is measured simply by η'/η . If $\eta'/\eta \geq 1$, there is no strength contrast, and the interface is fully coupled (Figure 5a). The resultant flow pattern is very similar to that of the analytical corner flow solution, except for the effects of slab curvature. A viscosity contrast of $\eta'/\eta = 10^{-2}$ leads to partial coupling over the length of the thin layer (Figure 5b), and $\eta'/\eta \leq 10^{-3}$ causes nearly complete decoupling (Figure 5c).

4. Model Results

4.1. Surface Heat Flow, Wedge Flow, and Temperature

[28] Most models in this section are of the type shown in Figure 4b, in which the interface layer extends throughout the model domain, and the depth of decoupling is thermally controlled. In warm-slab models, a thin-layer viscosity $\eta' \geq 3 \times 10^{19}$ Pa s leads to full coupling for practically the entire slab-mantle wedge interface (except for a tiny segment at the wedge tip) (Figure 6a). Decoupling occurs at lower η' values, and the maximum depth of decoupling increases with decreasing η' (Figures 6b, 6c, and 6d).

[29] The predicted surface heat flow patterns are compared with observations from northern Cascadia in Figure 7.

The heat flow data were obtained from Vancouver Island where the subducting slab is younger (6 Ma) and the slab dips slightly more steeply in the forearc region than in the model which is intended to represent a northern Cascadia average. For all four warm-slab models in Figure 6, the predicted surface heat flow seaward of the trench is slightly lower than the observed because of the older slab (8 Ma) in our model. The higher predicted values compared to the data from the trench to ~ 175 km landward are caused by the shallower slab dip used in our model. However, these differences have little effect on the mantle wedge thermal structure.

[30] The most important constraint from the surface heat flow observations is the change from the trend of landward decrease to landward increase. This change indicates where mantle material starts to participate in wedge flow and thus the maximum depth of decoupling. The abruptness of the heat flow rise observed in some locations where there is high data density [*Lewis et al.*, 1992; *Blackwell et al.*, 1990a, 1990b] is likely to be caused by local, near-surface processes such as magma emplacement associated with arc volcanism and cannot be accounted for in our large-scale modeling. Near-surface processes can greatly increase surface heat flow, but we cannot think of a mechanism for these processes to decrease surface heat flow systematically. Therefore, when using the heat flow values to constrain our large-scale models, we pay much more attention to explaining why the observed heat flows are low in most of the forearc region. The location of the initial rise predicted by the model with decoupling to ~ 70 or ~ 80 km (Figure 6b or 6c, respectively) is generally consistent with that of the observed pattern (Figure 7). Stronger coupling induces flow near the wedge tip, causes high temperature in the forearc mantle wedge, and therefore causes the heat flow rise to occur at a shorter distance from the trench (e.g., Figure 6a). The model with decoupling to ~ 120 km (Figure 6d) yields a heat flow pattern marginally consistent with observations, but the predicted temperature beneath the volcanic arc is too low for melt generation.

[31] Because both models in Figures 6b and 6c give a reasonable fit to heat flow observations, the choice between the two has to be based on their predicted mantle wedge temperature below the volcanic arc. For example, if the temperature is required to be greater than 1250°C , one may argue that the model in Figure 6b is a better choice. However, given the present large uncertainties in the interpretation of geochemical data to infer arc-mantle temperatures [*Kelemen et al.*, 2003], both models are equally

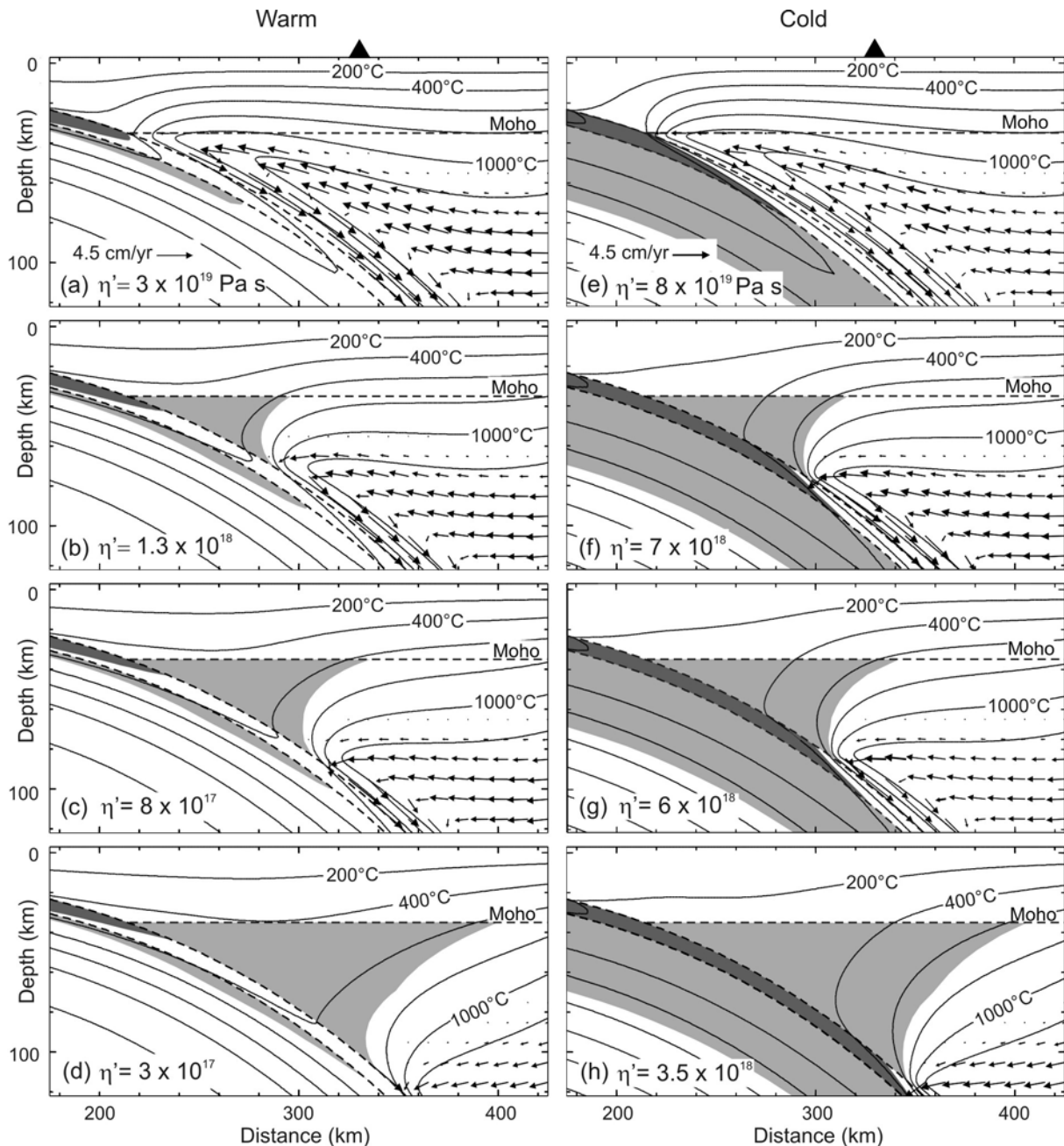


Figure 6. Temperature and flow velocities (arrows) in models with a dislocation-creep mantle wedge rheology. (a) Full coupling, (b) decoupling to ~ 70 km depth, (c) decoupling to ~ 80 km depth models shown in Figures 6b and 6c are preferred for Cascadia, and (d) decoupling to ~ 120 km depth in warm-slab models. (e) Full coupling, (f) decoupling to ~ 70 km depth, (g) decoupling to ~ 80 km depth, and (h) decoupling to ~ 120 km depth in cold-slab models. Each model is labeled with the interface layer viscosity (Pa s) used. Light grey in the mantle wedge and slab mantle indicates zones of antigorite stability. Dark grey and white in the subducting crust represent regions of high (>1 wt%) and low (≤ 1 wt%) H_2O contents, respectively. The boundary between them roughly represents the basalt-eclogite transformation. The transformation may be kinetically delayed in the lower subducting crust.

acceptable. Thus, the model shown in either Figure 6b or 6c can be considered our preferred model for northern Cascadia.

[32] For comparison, the results of cold-slab models are also shown in Figure 6. To ensure that the age of the incoming plate is the only difference in model set up, we use the same model geometry as shown in Figure 3. For the

same maximum depth of decoupling, the flow pattern in the mantle wedge is similar to that of a warm-slab model. The mantle material immediately above the old slab is colder than above a young slab, resulting in a slightly higher η_e in the mantle wedge. Because of the stronger mantle wedge, the layer viscosity that causes decoupling does not need be

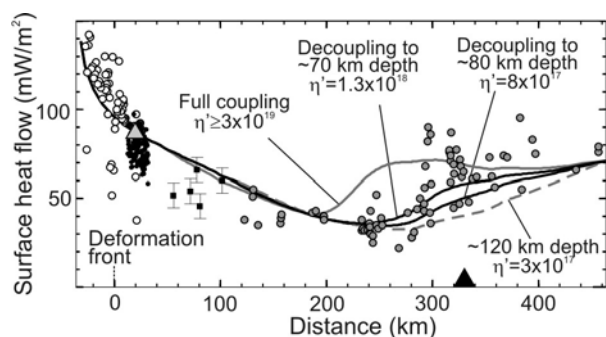


Figure 7. Surface heat flow for the warm slab models shown in Figure 6 compared with observations at northern Cascadia. Small black dots, white circles, squares, and the grey triangle are heat flow values obtained from bottom-simulating reflectors, marine probes, shelf wells, and an ODP borehole, respectively [Davis *et al.*, 1990; Lewis *et al.*, 1992; Hyndman *et al.*, 1993; Wang *et al.*, 1995]. Grey circles are heat flow observations compiled by Currie *et al.* [2004a]. The scattered very high values near the volcanic arc are affected by local near-surface processes and do not represent background heat flow. Each model is labeled with the interface layer viscosity (Pa s) as in Figure 6.

as low as for the warm-slab models. The geophysical meaning and implications of the layer viscosity will be discussed in section 4.3.

[33] Because the mantle wedge should be cold in the forearc as mentioned in section 1 yet also has to be sufficiently hot for melt generation beneath the volcanic arc, the models with decoupling to about 70–80 km depths, as shown in Figures 6b, 6c, 6f, and 6g, are considered representative of most subduction zones. Decoupling depths of 70–80 km have been used in thermal models of several different subduction zones constrained by heat flow and/or other geophysical observations [e.g., Furukawa, 1993; Peacock and Wang, 1999; van Keken *et al.*, 2002; Currie *et al.*, 2004a; Kneller *et al.*, 2005; Abers *et al.*, 2006].

[34] We find that the state of the mantle wedge flow tends to be bimodal: It either flows at a full rate compatible with slab velocity or is virtually stagnant (velocity < 0.01 cm/yr). Regardless of the thermal structure of the incoming plate, a reduced flow velocity due to decoupling leads to lower temperatures because conductive cooling due to the presence of the slab becomes more dominant as compared to convective transfer of heat from greater depths by wedge flow. The lower temperature causes a higher η_e , which means an increase in the strength contrast between the mantle wedge and the interface and thus further decoupling. This nonlinear feedback always leads to nearly complete stagnation above the decoupled interface, in contrast with an isoviscous mantle wedge that may flow at a reduced velocity above a weak interface (Figure 5b), and also in contrast with models with decoupling prescribed using a differential velocity (partial decoupling). The bimodal behavior is more clearly illustrated in Figure 8, which shows how the flow velocity at the base of the mantle wedge (top boundary of the thin layer) changes with depth. The velocity is virtually zero if the slab and mantle are decoupled but is the plate convergence velocity if they are coupled.

[35] The bimodal behavior allows some simplifications to be used in modeling practice. For example, the free-slip decoupling zone with a prescribed termination depth used by Furukawa [1993] and the “rigid corner” used by Peacock and Wang [1999], van Keken *et al.* [2002], and Currie *et al.* [2004a] are reasonable approximations since they all impose a sharp transition from no wedge flow to full-speed flow. Also, since most of the wedge above the zone of decoupling is stagnant, within a broad range, the rheological parameters used for this part of the wedge have little influence. It is the strong sensitivity to temperature and stress that gives rise to the sharp transition between the stagnant and flowing parts of the mantle wedge; the exact parameter values are not critical. This is why even the rigid corner model can be a reasonable approximation.

4.2. Slab Dehydration and Mantle Wedge Serpentinization

[36] Using the calculated thermal field and the pressure converted from depth (assuming a rock density of 3300 kg/m³), we outline two important petrological boundaries in Figure 6. The zones of antigorite stability in the mantle wedge and the subducting mantle are based on phase boundaries for wet peridotite provided by Schmidt and Poli [1998] (Figure 9a). The illustrated zones of stability in the mantle wedge and subducting mantle represents the maximum possible spatial extent of antigorite; how much antigorite is actually present depends on how much fluid is available. For example, antigorite as well as other hydrous minerals discussed in section 2 is expected to be most abundant along the base of the mantle wedge. The depths of basalt-eclogite transformation, approximately corresponding to the depths of peak dehydration of the subducting crust, are based on phase boundaries of H₂O-saturated basalt reported in the work of Hacker *et al.* [2003a] (Figure 9b). As explained by Hacker *et al.* [2003b], the transformation in the much more anhydrous lower crust is very likely to be kinetically delayed to greater

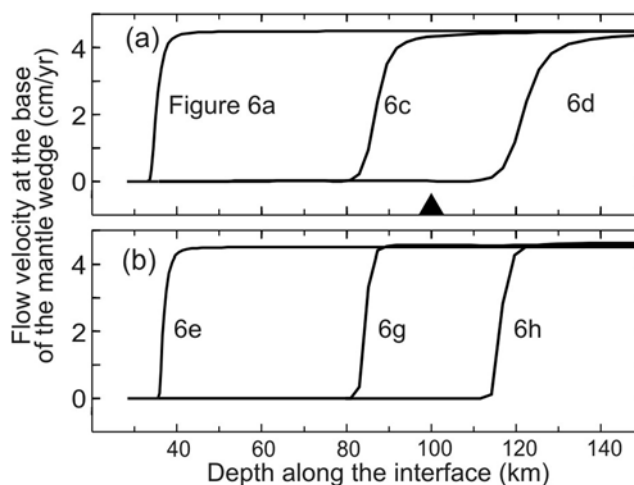


Figure 8. Flow velocity at the base of the mantle wedge. Approximate location of the volcanic arc is indicated using a solid triangle. (a) Warm-slab models shown in Figures 6a, 6c, and 6d. (b) Cold-slab models shown in Figures 6e, 6g, and 6h.

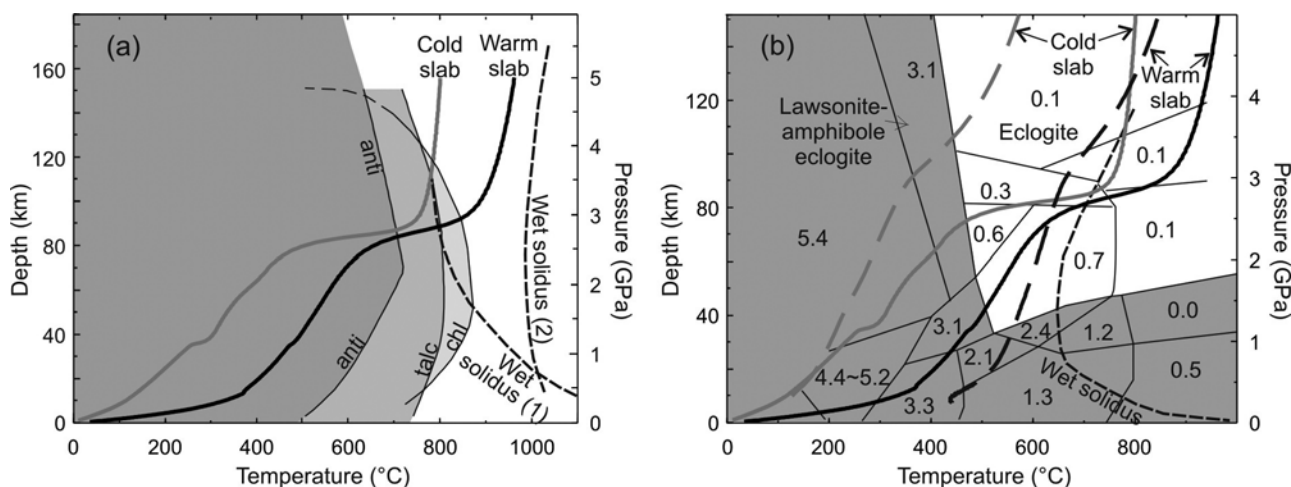


Figure 9. (a) Phase diagram of antigorite (anti), chlorite (chl), and talc. The antigorite and chlorite boundaries are from *Schmidt and Poli* [1998]. The talc boundary is from *Pawley and Wood* [1995]. The solidus for H₂O-saturated average mantle peridotite are from (1) *Grove et al.* [2006] and (2) *Schmidt and Poli* [1998]. (b) Metamorphic facies for basalt [*Hacker et al.*, 2003a]. Each facies is labeled with the maximum bound H₂O in wt % (facies names are given in the work of *Hacker et al.* [2003a]). The white area corresponds to the white area in the subducting crust in Figures 6 and 8. Temperatures along the slab surface for models in Figures 6c (warm slab) and 6g (cold slab) are shown with solid lines in both Figures 9a and 9b, and those along the bottom of the 7-km thick subducting crust with long-dashed lines in Figure 9b.

depths than shown in Figure 6. In the following discussions, we ignore fluids produced by the dehydration of subducted sediments. The total volume of sediments that are subducted to mantle wedge depths is usually very small as compare to that of the igneous crust.

[37] The degree of decoupling along the interface controls both the hydration of the mantle wedge and the dehydration of the slab. For the same maximum depth of decoupling, the warm-slab and cold-slab models have a similar zone of antigorite stability in the mantle wedge. Large differences are observed in the slab, however. With the same decoupling depth, dehydration of the subducting crust and mantle occurs at much greater depths in a cold slab than in a warm slab.

[38] Our preferred Cascadia model (Figure 6b or 6c) shows that slab dehydration peaks at shallow depths, being less than 50 km for the subducting crust and less than 100 km for the subducting mantle, shallower than those predicted by isoviscous mantle rheology which results in a cooler mantle wedge [e.g., *Hacker et al.*, 2003b]. *Bostock et al.* [2002] noticed an absence of wave-speed contrast across the plate interface deeper than about 45 km at southern Cascadia, where the thermal regime is expected to be similar to northern Cascadia, and inferred that it is caused by basalt-eclogite transformation in the subducting upper crust, increasing its wave speeds and thus diminishing its contrast with the overriding mantle wedge. This inference is consistent with our preferred Cascadia models. The shallow dehydration over the long history of subduction at Cascadia ensures large and sustained fluid supply for the hydration of the forearc mantle wedge corner. Therefore, the antigorite stability region in the mantle wedge shown in Figure 6b or 6c is expected to be substantially serpentinized. The model thus supports the inference of a high degree of mantle

wedge serpentinization from geophysical observations as mentioned in section 1.

[39] In the preferred cold-slab model (Figure 6f or 6g), the dehydration of the subducting crust peaks not beneath the stagnant mantle wedge but at larger depths. In northeast Japan, a typical cold-slab subduction zone, the results of high-resolution double-difference seismic tomography by *Tsuji et al.* [2007] show a low-wave-speed subducting crust down to ~80 km depth. In a reflectivity image obtained by *Kawakatsu and Watada* [2007] also for northeast Japan, the slab-surface reflector disappears at ~90 km depth. These results are consistent with the depths of basalt-eclogite transformation predicted by our preferred cold-slab models. The study by *Kawakatsu and Watada* [2007] shows the Moho reflector to extend to ~125 km depth, which can be interpreted as evidence for kinetically delayed transformation of the lower crust [*Hacker et al.*, 2003b]. In our preferred cold-slab models, the subducting mantle also undergoes little dehydration beneath the forearc because there is little change in its thermal state.

[40] Most of the fluid from the cold slab enters the warmer and flowing part of the mantle wedge where antigorite is no longer stable. Although the thermal and pressure conditions allow serpentinization in the stagnant part of the wedge, the availability of H₂O here is much less than for a warm slab. Porosity collapse of the subducted sediment and crust also releases fluid, but it is expected to occur at shallow depths (<~20–40 km) and provide little fluid to the mantle wedge except at ocean-ocean margins where the Moho of the overriding plate is only ~7 km below the seafloor. Therefore, the stagnant forearc wedge above a very cold slab at active continental margins should be relatively “dry.” Some hydrous minerals in the subducting crust will dehydrate and release some fluid before the

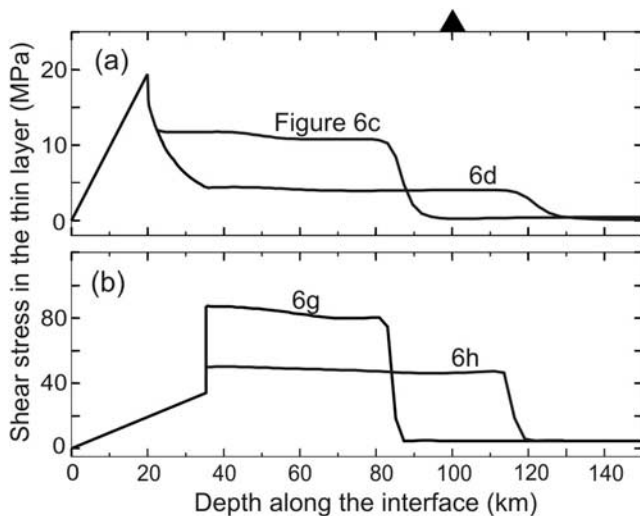


Figure 10. Shear stresses in the interface thin layer. Approximate location of the volcanic arc is indicated using a solid triangle. (a) Warm-slab models shown in Figures 6c and 6d. (b) Cold-slab models shown in Figures 6g and 6h.

dehydration reactions peak at the basalt-eclogite transformation [Hacker *et al.*, 2003b]. The small amounts of fluid released in this fashion may cause hydrous minerals to form along the base of the mantle wedge to weaken the subduction interface (see section 2) but is probably insufficient to cause a substantial degree of hydration in the stagnant forearc mantle wedge. In several places in northeast Japan, the mantle wedge corner has relatively high seismic wave speeds, indicative of a low degree of serpentinization [e.g., Zhao *et al.*, 1992; Nakajima *et al.*, 2001; Takahashi *et al.*, 2004; Miura *et al.*, 2005] and in sharp contrast with the warm-slab Cascadia subduction zone. However, at least in one location in northeast Japan, relatively low wave speeds were observed in the mantle wedge corner [Miura *et al.*, 2003]. If this is interpreted as evidence for serpentinization, the serpentinization is obviously rather localized and may be controlled by channelized upward migration of fluids.

[41] The availability of fluids in the forearc region depends also on the state of hydration of the incoming plate prior to subduction, but we expect that the difference in dehydration depths between warm and cold slabs provides the most important control. Although an old oceanic plate may be more hydrous than a very young plate [e.g., Jarrard, 2003], it withholds most of its water until the depth of 80–100 km.

[42] An important result of our modeling with a stress- and temperature-dependent rheology is that mantle wedge serpentinization occurs only in the forearc. For both warm- and cold-slab subduction zones, the mantle beneath the arc and back arc is too hot to be serpentinized. Relatively low seismic wave speeds are observed immediately above the subducting slab beneath the arc and back arc in northeast Japan [e.g., Hattori and Guillot, 2003; Kawakatsu and Watada, 2007]. On the basis of previous thermal models with an isoviscous mantle wedge [e.g., Iwamori, 1998; Peacock and Wang, 1999], these observations could be interpreted as to indicate the presence of serpentine [e.g., Kawakatsu and Watada, 2007]. With a more realistic

nonlinear mantle wedge rheology, these observations have to be interpreted differently. For example, they may indicate trapped fluids or even the presence of melts just about the slab.

[43] At cold-slab ocean-ocean subduction zones, such as Mariana, the overriding forearc mantle is situated at a very shallow depth beneath the thin oceanic crust. Although slab dehydration is minimal at such depths, the shallow part of the forearc mantle wedge can still be hydrated by fluids released from porosity collapse in the subducted sediment and fractured igneous crust. This explains the source of serpentinite deposits that were emplaced by serpentinite mud volcanoes or by processes of large-scale faulting and rifting in the Mariana forearc [Fryer, 1996].

4.3. Stress Along the Interface

[44] To understand the nature of the coupling and decoupling as portrayed in our models, it is necessary to examine the distribution of shear stress along the interface (Figure 10). For the examples shown in Figure 10, the linear increase in the shallowest part results from Coulomb friction used to calculate Q_{FH} , as explained in section 3.2. What is the most relevant for this study is the stress along the slab-mantle wedge contact which is determined by the viscosity and shear strain rate of the thin layer along the interface.

[45] The stress distribution may appear counterintuitive in that the decoupled part of the interface has a higher stress than the fully coupled part further downdip. For example, in the preferred Cascadia model (Figure 10a), the stress along the decoupled part of the interface from 35 km to 80 km depths is about 14 MPa but sharply decreases to about 1 MPa along the coupled deeper part. This is the best demonstration that coupling and decoupling is controlled by the strength contrast between the interface and the mantle wedge, not by the absolute strength of the interface alone. Across the downdip transition from decoupling to coupling, the stress along the interface decreases by about one order of magnitude, but the viscous strength of the overlying mantle wedge decreases by several orders of magnitude because of the temperature- and stress-dependent rheology. In the warmer (roughly $>800^{\circ}\text{C}$) part of the mantle wedge, the effective viscosity is so low that the shear stress is everywhere less than 1 MPa (results not shown), as is also shown in the models of Kneller *et al.* [2005]. Beneath the volcanic arc, the presence of melts is expected to further weaken the mantle wedge material.

[46] Some limit on the level of shear stress along the slab-mantle wedge interface can be placed on the basis of the state of stress in the upper plate. In the Cascadia forearc, earthquake focal mechanisms and other stress indicators suggest a lack of a strong margin-normal compression [Wang and He, 1999]. If all the margin-normal compression is caused by frictional coupling along the shallowest part of the Cascadia megathrust (the seismogenic portion), an effective coefficient of fault friction μ' less than 0.08 can explain the observed degree of compression [Wang and He, 1999]. In northeast Japan, where a cold slab is being subducted, there is strong margin-normal compression, but even this compression can be explained using a weak subduction fault that extends to 50 km depth, consistent with the observed depth extent of the seismogenic zone

[Wang and Suyehiro, 1999]. In northeast Japan, large shear stress further downdip is not required, although it cannot be excluded. The horizontal component of the shear stress along the base of the stagnant mantle wedge that exerts margin-normal compression on the upper plate is about 70% of what is shown in Figure 10 (solid lines), given the dip of the interface. This, combined with the shear stress along the updip seismogenic portion, would give a margin-normal compression somewhat higher than required by forearc stress observations, especially for the Cascadia case.

[47] We argue that the values shown in Figure 10 are upper limits, and the actual values in real subduction zones are very likely to be much lower. We have tried to perturb the preferred models of Figures 6b, 6c, 6f, and 6g by increasing or decreasing the strength (i.e., thin-layer viscosity) of the decoupled part of the interface while keeping the rest of the interface unchanged. If the decoupled interface is any stronger, that is, if the interface stress is higher than shown in Figure 10, decoupling will be terminated at a shallower depth. However, if the decoupled interface becomes a few times as weak, the depth of decoupling is not significantly affected. In a real subduction zone, the decoupled part of the interface is expected to have a tendency for further weakening because of continuing fluid supply from the slab and the increasing degree of hydration of the base of the stagnant mantle wedge. Therefore, the stress along the decoupled interface is also expected to be lower than shown in Figure 10.

[48] It is worth mentioning the role of shear heating along the interface in limiting the stress. We have also tested models without including viscous shear heating (results not shown). In those models, the η_e values immediately above the slab are much higher. As a result, the viscosities of the thin layer required to produce flow and temperature patterns nearly identical to those shown in Figure 6 are orders of magnitude higher, and the shear stresses along the interface are unacceptably high.

[49] In this work, we have shown that interface weakening and the temperature-dependent rheology of the mantle wedge material have a first-order control on the termination depth of decoupling, but we have not explored other feedback mechanisms. The relatively narrow range of decoupling depth in nature as discussed in section 4.1 suggests a self-regulating process characterized by an inherent scale length. The scale length is probably ultimately controlled by the heat budget of the back arc, although the exact mechanism is yet to be identified. Back arc heat flows for most subduction zones are about 80 mW/m^2 and likely to be governed by a common process of small scale convection [Currie and Hyndman, 2006]. This probably determines the amount of heat supply into the arc and forearc region and thus the weakening of the mantle wedge material that terminates decoupling.

5. Discussion

5.1. Intraslab Earthquakes and Nonvolcanic Tremor

[50] Fluids released during slab dehydration may greatly elevate pore fluid pressure within the slab to facilitate seismic failure [Kirby *et al.*, 1996]. This process of “dehydration embrittlement” (a term originally used to describe a laboratory observation that fluid release causes an immedi-

ate change from ductile to brittle deformation) is expected to work in both the subducting crust and subducting mantle. In our preferred model for northern Cascadia (Figure 6b or 6c), the slab becomes fairly anhydrous at 100 km depth, in agreement with the observed depth limit of Cascadia intraslab earthquakes [Ludwin *et al.*, 1991; Hacker *et al.*, 2003b].

[51] Our models confirm some general findings of Peacock and Wang [1999] and Hacker *et al.* [2003b] regarding the seismological consequences of slab petrology of warm- versus cold-slab subduction based on simpler models of isoviscous mantle wedge. However, as shown in the work of van Keken *et al.* [2002], Peacock *et al.* [2005], Abers *et al.* [2006], and all published models based on the dislocation-creep mantle rheology, if decoupling is confined to the forearc region, dehydration of the subducting crust peaks at depths shallower than 120 km regardless of the age of the subducting plate (e.g., Figures 6g and 9b), contradicting findings based on isoviscous wedge models. This poses a challenge to explaining deeper intraslab earthquakes that occur in the subducting crust at cold-slab subduction zones. For these earthquakes to occur via dehydration embrittlement, processes like dehydration of high-temperature hydrous phases [e.g., Schmidt and Poli, 1998], kinetically delayed dehydration, sustained high pore fluid pressure due to extremely low permeability, or migration of fluid from dehydrating slab mantle to the slab crust have to be invoked. Alternative mechanisms such as shear-heating instability are also worth exploring.

[52] At northern Cascadia, non-volcanic tremor and associated silent slip of the subduction interface episodically occur in the region around the tip of the mantle wedge (Figure 1) [Dragert *et al.*, 2001; Rogers and Dragert, 2003]. Similar phenomena are observed at the Nankai subduction zone [Obara, 2002; Hirose and Obara, 2005], where the slab is also young and warm and evidence for mantle wedge serpentinization is also strong. It is suggested that the tremor and slip may be related to free fluids released from the slab, although the exact mechanism is unknown [Obara, 2002; Kao *et al.*, 2005; Shelly *et al.*, 2007]. The availability of free fluids depends on how much of the fluids is consumed in serpentinizing the mantle wedge. On the basis of seismic tomography at northern Cascadia, K. Ramachandran and R. D. Hyndman (submitted manuscript, 2008) inferred that the degree of mantle wedge serpentinization decreases landward from the tip of the wedge. Although a typical serpentinization of $\sim 15\%$ is inferred from seismic velocity studies of subduction zones where there is evidence for mantle wedge serpentinization [Carlson and Miller, 2003], the degree of serpentinization at the wedge tip may be very high, conceivably approaching 100% given the diminishing vertical dimension of the wedge. Ample free fluids should be available in this region because they are not rapidly consumed by further serpentinization. This may explain why non-volcanic tremor and slip events occur at and near the wedge tip. Similar episodic tremor and slip events are rare in cold-slab subduction zones, and this may be due to the shortage of fluid supply in the forearc region.

5.2. Arc Volcanism

[53] The temperature required to generate melts beneath the volcanic arc as reported in the literature has varied

dramatically [Grove *et al.*, 2006], but there is no doubt that the addition of aqueous fluids is required. In the cold-slab model (Figure 6f or 6g), crustal dehydration peaks beneath the arc, providing ample fluids for melt generation. But in the warm-slab model (Figure 6b or 6c), dehydration peaks “prematurely” at shallow depths, explaining the feeble arc volcanism at Cascadia. However, although volcanic activity at warm-slab subduction zones is generally low [Kirby *et al.*, 1996], it does occur. How fluids are transported to the region below the arc in this type of subduction zone is an important question. One possibility is that some high-temperature hydrous minerals in the slab can survive to large depths. Other proposed mechanisms resort to transporting fluids by mantle wedge flow, that is, some hydrous minerals in the mantle wedge, such as chlorite which contains ~13 wt% H₂O, may travel with the downdip wedge flow and be dehydrated beneath the volcanic arc [Tatsumi and Eggins, 1995]. Our models suggest that both mechanisms can be at work. In the model of Figure 6b or 6c, antigorite in the subducting mantle can be stable to a depth of ~100 km. In the same model, although antigorite in the mantle wedge is not stable below the maximum depth of decoupling, the zone of chlorite stability just above the slab extends down to about 90 km depth as can be inferred from Figure 9a. Therefore, potentially the mantle-wedge flow can transport chlorite down to this depth, providing some fluid for limited magma generation. It is also suggested that tectonic erosion can cause slivers of serpentinized mantle material above the slab to be dragged downdip to greater depths to dehydrate beneath the arc region [e.g., Tonarini *et al.* 2007].

[54] On the basis of geochemical signatures of arc lavas, Kelemen *et al.* [2003] argue that partial melting of the subducted sediment and the topmost part of the igneous crust commonly occurs. In our preferred warm- and cold-slab models, the temperature of the slab along the slab surface intersects the wet solidus of basalt (Figure 9b). Although there are large uncertainties in the wet solidus temperature, our results show that the upper most part of the subducting crust and subducted sediment, if present, can potentially undergo partial melting, even in cold-slab subduction zones. Other thermal modeling studies involving the temperature- and stress-dependent mantle wedge rheology show similar results [e.g., Peacock *et al.*, 2005]. In contrast, models with an isoviscous mantle wedge show cooler thermal conditions and thus no slab melting except for end-member warm-slab subduction zones [e.g., Hacker *et al.*, 2003b].

[55] The average depth to the top of the slab surface beneath arc volcanoes is about 110 km, with a significant scatter [England *et al.*, 2004; Syracuse and Abers, 2006]. England *et al.* [2004] tried to explain a correlation between the location of the arc relative to the slab with the descent speed of the slab. The reason for the preferred arc location of about 110 km over the slab remains an enigma. Pressure-dependent dehydration reactions in the subducting slab do not seem to be the primary control, since there are no known major dehydration boundaries at the pressure of about 110 km depth (Figure 9). As shown in our study, the termination depth of interface decoupling determines the thermal structure of the mantle wedge and thus affect arc location. The inherent scale length mentioned in section

4.3 appears to control both the maximum depth of decoupling and the arc location.

5.3. Seismic Anisotropy in the Forearc Mantle Wedge

[56] The stagnant forearc mantle wedge seen in our models may have some implications for the interpretation of seismic anisotropy in this environment. In the upper mantle, lattice preferred orientation (LPO) of olivine develops during shear deformation, and the resultant seismic anisotropy causes orthogonal components of shear waves to travel at different velocities. Convergence-parallel fast direction is commonly observed in subduction zone upper mantle and is interpreted to indicate mantle flow and thus the shear direction being aligned with plate convergence.

[57] However, the fast direction in the forearc mantle wedge at many subduction zones is observed to be normal to the convergence direction, for which there are several interpretations [Wiens and Smith, 2003]. One hypothesis is that in a “wet” condition at low temperature and high shear, the LPO of olivine results in a fast direction that is normal to the convergence direction (B-type olivine fabric) [Jung and Karato, 2001]. In contrast to conventional views, this mechanism does not require the mantle flow to change from convergence-parallel beneath the arc to margin-parallel in the forearc. There are some outstanding issues, though.

[58] The first issue is whether there is significant shear deformation in the stagnant mantle wedge. In the models of Kneller *et al.* [2005, 2007], a velocity of about 3% of the plate convergence rate is assigned to the base of the forearc mantle wedge. The resultant slow “corner flow” creates enough shear deformation for the presence of the B-type fabric. Using a weak layer along the interface to simulate a condition of stress coupling, we have shown that there is little ongoing shear deformation in the stagnant wedge above the decoupled interface. One possibility is that the B-type fabric had been generated by deformation prior to the interface became decoupled and since “locked” in the rocks.

[59] The second issue is how to explain the presence of arc-parallel fast direction observed in the arc-back arc mantle wedge of some subduction zones, such as Tonga [Smith *et al.*, 2001], Ryukyu [Long and van der Hilst, 2006], and Mariana [Pozgay *et al.*, 2007]. Beneath the arc and the back arc, temperatures are too high and stresses are too low to allow the formation of B-type olivine fabric.

[60] The third issue is how to explain the convergence-parallel fast direction reported for warm-slab subduction zones such as Cascadia and Nankai [Currie *et al.*, 2004b; Tono, 2006]. What causes the convergence-parallel fast direction in a serpentinized mantle wedge? Whatever mechanism that explains the anisotropy in cold-slab forearcs must explain why a warm-slab forearc behaves so differently. This is an important subject for future studies.

6. Conclusions

[61] Using a thin layer of uniform viscosity along the subduction interface and the dislocation-creep rheology for the mantle wedge, we have numerically investigated the effect of interface decoupling on mantle wedge flow and subduction zone thermal regime. For a given layer viscosity,

the maximum depth of decoupling in our model is thermally controlled. The effective viscosity of the mantle wedge decreases with increasing depth, and the transition from decoupling to coupling along the interface occurs where the mantle wedge viscosity becomes equal to or less than the layer viscosity. The thin layer simulates a stress condition along the interface and is an improvement over methods used to represent decoupling in previously published models of similar type. On the basis of the results of the finite element models, we draw the following conclusions.

[62] 1. Flow in the forearc mantle wedge shows a bimodal behavior due to the nonlinear mantle rheology. Depending on the degree of decoupling along the interface, the base of the mantle wedge either flows at the slab velocity or almost does not flow at all. Over a weakened interface, the forearc wedge becomes stagnant. Varying the strength of the interface changes the maximum depth of decoupling but does not change the bimodal wedge flow behavior. The computed downdip transition from decoupling to coupling is abrupt, such that the model results are similar to those obtained with a kinematically imposed maximum depth of decoupling.

[63] 2. Because of the bimodal flow behavior, the spatial transition between the thermal states of the seaward stagnant part and the landward, deeper flowing part of the mantle wedge is rather abrupt. The cold stagnant part gives low heat flow at the surface; the hot flowing part gives high heat flow and maintains the high temperature and heat source required by arc volcanism. The observed change in surface heat flow pattern from landward decrease to landward increase in the forearc is controlled by the location of the transition from decoupling to coupling along the subduction interface. The abruptness of the increase observed in some places is likely to be caused by near-surface processes that are not considered in this study.

[64] 3. The stagnation and consequent cool condition of the forearc mantle wedge provide a stable environment for serpentinization. With interface decoupling to a depth of about 70–80 km, models of warm-slab and cold-slab subduction yield a similar region of antigorite stability in the mantle wedge. However, these models predict very different abundance of fluid supply into the forearc wedge. Other conditions being equal, a very warm slab such as at Cascadia is predicted to release most of its H₂O in the forearc region and cause a high degree of serpentinization in the mantle wedge, but a very cold slab similar to that of northeast Japan is predicted to withhold most of its H₂O until farther downdip and result in a lower degree of forearc serpentinization.

[65] 4. Mantle wedge serpentinization can occur only in the forearc. Thermal models with an isoviscous mantle wedge show that the mantle immediately above the slab is cold enough to be serpentinized even beneath the volcanic arc. However, models with the dislocation-creep mantle rheology show that antigorite stability extends down only to the maximum depth of decoupling, which, in accordance with heat flow observations and the mantle wedge temperature required for arc volcanism, must be located in the forearc region.

[66] 5. The shallow depth of slab dehydration in our preferred Cascadia model (Figure 6b or 6c) and the observed shallow termination of intraslab seismicity at Cascadia

together support the dehydration embrittlement hypothesis for intraslab earthquakes. The shallow dehydration can explain the low level of volcanic activity of the Cascades, but the model also shows that small amounts of fluids can be transported down to the arc area by the subducting mantle or mantle wedge flow to enable some feeble arc volcanism. The predicted ample fluid supply from slab dehydration in the forearc is consistent with the geophysically inferred presence of a highly serpentinized forearc mantle wedge.

[67] 6. Similar to all other models based on the dislocation-creep mantle rheology, our preferred cold-slab model (Figure 6f or 6g) predicts that the dehydration of the subducting crust peaks at depths shallower than 120 km, making it difficult to use crustal dehydration of common hydrous minerals under thermodynamic equilibrium to explain near-slab-surface earthquakes that are observed to occur to much greater depths in many cold-slab subduction zones.

[68] 7. The strong tendency for the forearc mantle wedge above the decoupled interface to become stagnant creates difficulty for the explanation of margin-parallel fast directions constrained by shear-wave-splitting analyses in many subduction zones in terms of the B-type olivine fabric which requires rather large shear deformation.

[69] 8. Decoupling is a reflection of the strength contrast between the interface and the mantle wedge. Although a weaker interface leads to a greater maximum depth of decoupling, the downdip transition from decoupling to coupling may not be accompanied with a stress increase along the interface. On the contrary, if the strength of the interface is assumed to be uniform, the stress along the coupled deeper part of the interface is an order of magnitude lower than the decoupled shallower part. This is because of the extreme sensitivity of the effective viscosity of the mantle wedge to temperature. We consider the level of stress along the decoupled interface in our preferred models to represent an upper limit.

[70] 9. The configuration of the shallow subduction zone system indicates an inherent scale length. Decoupling must terminate around the landward edge of the forearc, but the exact mechanism of the termination is yet to be identified.

[71] **Acknowledgments.** Discussions with M. Bostock, C. Currie, E. Davis, H. Dick, B. Hacker, R. Hino, K. Kelley, S. Kirby, E. Kneller, and D. Moore are greatly appreciated. C. Currie and P. van Keken painstakingly compared the performance of PGTherm with other computing codes in a community benchmarking exercise (www.geo.lsa.umich.edu/~keken/subduction/benchmark). We thank J. Townend, G. Rogers, P. van Keken, and an anonymous reviewer for their valuable comments on earlier versions of the manuscript. Geological Survey of Canada contribution 20070333.

References

- Abers, G. A., P. E. van Keken, E. A. Kneller, A. Ferris, and J. C. Stachnik (2006), The thermal structure of subduction zones constrained by seismic imaging: Implications for slab dehydration and wedge flow, *Earth Planet. Sci. Lett.*, *241*, 387–397.
- Batchelor, G. K. (1967), *An Introduction to Fluid Dynamics*, 615 pp., Cambridge Univ. Press, New York.
- Bebout, G. E., and M. D. Barton (1989), Fluid flow and metasomatism in a subduction zone hydrothermal system: Catalina Schist terrane, California, *Geology*, *17*, 976–980.
- Blackwell, D. D., J. L. Steele, M. K. Frohme, D. F. Murphey, G. R. Priest, and G. L. Black (1990a), Heat flow in the Oregon Cascade Range and its correlation with regional gravity, Curie point depths, and geology, *J. Geophys. Res.*, *100*, 15,303–15,316.

- Blackwell, D. D., J. L. Steele, S. Kelley, and M. A. Korosec (1990b), Heat flow in the State of Washington and thermal conditions in the Cascade Range, *J. Geophys. Res.*, *95*, 19,495–19,516.
- Blakely, R. J., T. M. Brocher, and R. E. Wells (2005), Subduction-zone magnetic anomalies and implications for hydrated forearc mantle, *Geology*, *33*, 445–448.
- Bostock, M. G., R. D. Hyndman, S. Rondenary, and S. M. Peacock (2002), An inverted continental Moho and serpentinization of the forearc mantle, *Nature*, *417*, 536–538.
- Brocher, T. M., R. Parsons, A. M. Trehu, S. M. Snelson, and M. A. Fisher (2003), Seismic evidence for widespread serpentinized forearc upper mantle along the Cascadia margin, *Geology*, *31*, 267–270.
- Carlson, R. L., and D. J. Miller (2003), Mantle wedge water contents estimated from seismic velocities in partially serpentinized peridotites, *Geophys. Res. Lett.*, *30*(5), 1250, doi:10.1029/2002GL016600.
- Chen, Y., and W. J. Morgan (1990), A nonlinear rheology model for mid-ocean ridge axis topography, *J. Geophys. Res.*, *95*, 17,583–17,604.
- Christensen, N. I. (1996), Poisson's ratio and crustal seismology, *J. Geophys. Res.*, *101*(B2), 3139–3156.
- Christensen, N. I. (2004), Serpentinized peridotites, and seismology, *Int. Geol. Rev.*, *46*, 795–816.
- Conder, J. A. (2005), A case for hot slab surface temperatures in numerical viscous flow models of subduction zones with improved fault zone parameterization, *Earth Planet. Sci. Lett.*, *149*, 155–164.
- Currie, C. A. (2004), The thermal structure of subduction zones and back-arc, Ph.D. thesis, 267 pp., Univ. of Victoria, Victoria, B. C., Canada.
- Currie, C. A., and R. D. Hyndman (2006), The thermal structure of subduction zone back arcs, *J. Geophys. Res.*, *111*, B08404, doi:10.1029/2005JB004024.
- Currie, C. A., K. Wang, R. D. Hyndman, and J. He (2004a), The thermal effects of steady-state slab-driven mantle flow above a subducting plate: The Cascadia subduction zone and back arc, *Earth Planet. Sci. Lett.*, *223*, 35–48.
- Currie, C. A., J. F. Cassidy, R. D. Hyndman, and M. G. Bostock (2004b), Shear wave anisotropy beneath the Cascadia subduction zone and western North American craton, *Geophys. J. Int.*, *157*, 341–353.
- Davis, E. E., R. D. Hyndman, and H. Villinger (1990), Rates of fluid expulsion across the northern Cascadia accretionary prism: Constraints from new heat flow and multichannel seismic reflection data, *J. Geophys. Res.*, *95*, 8869–8889.
- DeShon, H. R., and S. Y. Schwartz (2004), Evidence for serpentinization of the forearc mantle wedge along the Nicoya Peninsula, Costa Rica, *Geophys. Res. Lett.*, *31*, L21611, doi:10.1029/2004GL021179.
- Dragert, H., K. Wang, and T. S. James (2001), A silent slip event on the deeper Cascadia subduction interface, *Science*, *292*, 1525–1528.
- England, P., R. Engdahl, and W. Thatcher (2004), Systematic variation in the depths of slabs beneath arc volcanoes, *Geophys. J. Int.*, *156*, 377–408.
- Evans, B. W. (1977), Metamorphism of alpine peridotite and serpentinite, *Ann. Rev. Earth Planet. Sci.*, *5*, 397–447.
- Evans, B. W. (2004), The serpentine multisystem revised: Chrysotile is metastable, *Int. Geol. Rev.*, *46*, 479–506.
- Fryer, P. (1996), Evolution of the Mariana convergent plate margin system, *Rev. Geophys.*, *34*, 89–125.
- Furukawa, Y. (1993), Depth of the decoupling plate interface and thermal structure under arcs, *J. Geophys. Res.*, *98*, 20,005–20,013.
- Furukawa, Y., and S. Uyeda (1989), Thermal state under the Tohoku arc with consideration of crustal heat generation, *Tectonophysics*, *164*, 175–187.
- Goto, A., and Y. Tatsumi (1990), Stability of chlorite in the upper mantle, *Am. Mineral.*, *75*, 105–108.
- Graeber, F. M., and G. Asch (1999), Three-dimensional models of P wave velocity and P-to-S ratio in the southern central Andes by simultaneous inversion of local earthquake data, *J. Geophys. Res.*, *104*, 20,237–20,256.
- Grove, T. L., N. Chatterjee, S. W. Parman, and E. Medard (2006), The influence of H₂O on mantle wedge melting, *Earth Planet. Sci. Lett.*, *249*, 74–89.
- Hacker, B. R., G. A. Abers, and S. M. Peacock (2003a), Subduction factory: 1. Theoretical mineralogy, densities, seismic wave speeds, and H₂O contents, *J. Geophys. Res.*, *108*(B1), 2029, doi:10.1029/2001JB001127.
- Hacker, B. R., S. M. Peacock, G. A. Abers, and S. D. Holloway (2003b), Subduction factory: 2. Are intermediate-depth earthquakes in subducting slabs linked to metamorphic dehydration?, *J. Geophys. Res.*, *108*(B1), 2030, doi:10.1029/2001JB001129.
- Hasegawa, A., S. Horiuchi, and N. Umino (1994), Seismic structure of the northeastern Japan convergent margin: A synthesis, *J. Geophys. Res.*, *99*, 22,295–22,311.
- Hattori, K. H., and S. Guillot (2003), Volcanic fronts form as a consequence of serpentinite dehydration in the forearc mantle wedge, *Geology*, *31*, 525–528.
- Hirose, H., and K. Obara (2005), Repeating short- and long-term slow slip events with deep tremor activity around the Bungo channel region, Southwest Japan, *Earth Planets Space*, *57*, 961–972.
- Hirth, G., and D. Kohlstedt (2003), Rheology of the upper mantle and the mantle wedge: A view from the Experimentalists, in *Inside the Subduction Factory*, *Geophys. Monogr. Ser.*, vol. 138, edited by J. Eiler, pp. 83–105, AGU, Washington D. C.
- Hyndman, R. D., and S. M. Peacock (2003), Serpentinization of the forearc mantle, *Earth. Planet. Sci. Lett.*, *212*, 417–432.
- Hyndman, R. D., K. Wang, T. Yuan, and G. D. Spence (1993), Tectonic sediment thickening, fluid expulsion, and the thermal regime of subduction zone accretionary prisms: The Cascadia margin off Vancouver Island, *J. Geophys. Res.*, *98*, 21,865–21,876.
- Ito, E., and T. Katsura (1989), A temperature profile of the mantle transition zone, *Geophys. Res. Lett.*, *16*, 425–428.
- Iwamori, H. (1998), Transportation of H₂O and melting in subduction zones, *Earth. Planet. Sci. Lett.*, *160*, 65–80.
- Jarrard, R. D. (2003), Subduction fluxes of water, carbon dioxide, chlorine, and potassium, *Geochem. Geophys. Geosyst.*, *4*(5), 8905, doi:10.1029/2002GC000392.
- Jung, H., and S. Karato (2001), Water-induced fabric transitions in olivine, *Science*, *293*, 1460–1463.
- Kamiya, S., and Y. Kobayashi (2000), Seismological evidence for existence of serpentinized wedge mantle, *Geophys. Res. Lett.*, *27*, 819–822.
- Kao, H., S. J. Shan, H. Dragert, G. Rogers, J. F. Cassidy, and K. Ramachandran (2005), Depth distribution of seismic tremors along the northern Cascadia margin, *Nature*, *436*, 841–844.
- Karato, S., and P. Wu (1993), Rheology of the upper mantle: A synthesis, *Science*, *260*, 771–778.
- Kawakatsu, H., and S. Watada (2007), Seismic evidence for deep-water transportation in the mantle, *Science*, *316*, 1468–1471.
- Kirby, S. H., E. R. Engdahl, and R. Denlinger (1996), Intermediate-depth intraslab earthquakes and arc volcanism as physical expressions of crustal and uppermost mantle metamorphism in subducting slabs, in *Subduction: Top to Bottom*, *Geophys. Monogr. Ser.*, vol. 96, edited by G. E. Bebout et al., pp. 195–214, AGU, Washington, D. C.
- Kelemen, P. B., J. Rilling, E. M. Parmentier, L. Mehl, and B. R. Hacker (2003), Thermal structure due to solid-state flow in the mantle wedge beneath arcs, in *Inside the Subduction Factory*, *Geophys. Monogr. Ser.*, vol. 138, edited by J. Eiler, pp. 293–311, AGU, Washington D. C.
- Kneller, E. A., P. E. van Keken, S. Karato, and J. Park (2005), B-type olivine fabric in the mantle wedge: Insights from high-resolution non-Newtonian subduction zone models, *Earth Planet. Sci. Lett.*, *237*, 781–797.
- Kneller, E. A., P. E. van Keken, I. Katayama, and S. Karato (2007), Stress, strain, and B-type olivine fabric in the fore-arc mantle: Sensitivity tests using high-resolution steady-state subduction zone models, *J. Geophys. Res.*, *112*, B04406, doi:10.1029/2006JB004544.
- Lewis, T. J., W. H. Bentkowski, and R. D. Hyndman (1992), Crustal temperatures near the Lithoprobe Southern Canadian Cordillera transect, *Can. J. Earth Sci.*, *29*, 1197–1214.
- Long, M. D., and R. D. van der Hilst (2006), Shear wave splitting from local events beneath the Ryukyu arc: Trench-parallel anisotropy in the mantle wedge, *Phys. Earth Planet. Inter.*, *155*, 300–312.
- Ludwin, R. S., C. S. Weaver, and R. S. Crosson (1991), Seismicity of Washington and Oregon, in *Neotectonics of North America, Decade of North American Geology*, vol. GSMV-1, edited by D. B. Slemmons et al., pp. 77–98, Geol. Soc. of Am., Boulder, Colo.
- Miura, S., S. Kodaira, A. Nakanishi, T. Tsuru, M. Takahashi, N. Hirata, and Y. Kaneda (2003), Structural characteristics controlling the seismicity of southern Japan Trench fore-arc region, revealed by ocean bottom seismographic data, *Tectonophysics*, *323*, 79–102.
- Miura, S., N. Takahashi, A. Nakanishi, T. Tsuru, S. Kodaira, and Y. Kaneda (2005), Structural characteristics off Miyagi forearc region, the Japan Trench seismogenic zone, deduced from a wide-angle reflection and refraction study, *Tectonophysics*, *407*, 165–188.
- Morrow, C. A., D. E. Moore, and D. A. Lockner (2000), The effect of mineral bond strength and adsorbed water on fault gouge frictional strength, *Geophys. Res. Lett.*, *27*, 815–818.
- Nakajima, J., T. Matsuzawa, A. Hasegawa, and D. Zhao (2001), Three-dimensional structure of V_p, V_s, and V_p/V_s beneath northeastern Japan: Implications for arc magmatism and fluids, *J. Geophys. Res.*, *106*, 21,843–21,858.
- Obara, K. (2002), Nonvolcanic deep tremor associated with subduction in Southwest Japan, *Science*, *296*, 1679–1681.
- Pawley, A. R., and B. J. Wood (1995), The high-pressure stability of talc and 10 Å phase: Potential storage sites for H₂O in subduction zones, *Am. Mineral.*, *80*, 998–1003.

- Peacock, S. M. (1987), Serpentinization and infiltration metasomatism in the Trinity peridotite, Klamath province, northern California: Implications for subduction zones, *Contrib. Mineral. Petrol.*, *95*, 55–70.
- Peacock, S. M., and R. D. Hyndman (1999), Hydrous minerals in the mantle wedge and the maximum depth of subduction thrust earthquakes, *Geophys. Res. Lett.*, *26*, 2517–2520.
- Peacock, S. M., and K. Wang (1999), Seismic consequences of warm versus cool subduction metamorphism: Examples from southwest and northeast Japan, *Science*, *286*, 937–939.
- Peacock, S. M., P. E. van Keken, S. D. Holloway, B. R. Hacker, G. A. Abers, and R. L. Fergason (2005), Thermal structure of the Costa Rica–Nicaragua subduction zone, *Phys. Earth Planet. Inter.*, *149*, 187–200.
- Pozgay, S. H., D. A. Wiens, J. A. Conder, H. Shiobara, and H. Sugioka (2007), Complex mantle flow in the Mariana subduction system: Evidence from shear wave splitting, *Geophys. J. Int.*, *170*, 371–386.
- Ramachandran, K., S. E. Doss, G. D. Spence, R. D. Hyndman, and T. M. Brocher (2005), Forearc structure beneath southwestern British Columbia: A three-dimensional tomographic velocity model, *J. Geophys. Res.*, *110*, B02303, doi:10.1029/2004JB003258.
- Ranalli, G. (1995), *Rheology of the Earth*, 2nd ed., 413 pp., Chapman and Hall, New York.
- Rogers, G., and H. Dragert (2003), Episodic tremor and slip on the Cascadia subduction zone: The chatter of silent slip, *Science*, *300*, 1942–1943.
- Schmidt, M. W., and S. Poli (1998), Experimentally based water budgets for dehydrating slabs and consequences for arc magma generation, *Earth Planet. Sci. Lett.*, *163*, 361–379.
- Seno, T., D. Zhao, Y. Kobayashi, and M. Nakamura (2001), Dehydration of serpentinized mantle: Seismic evidence from Southwest Japan, *Earth Planets Space*, *53*, 861–871.
- Shelly, D. R., G. C. Beroza, and S. Ide (2007), Non-volcanic tremor and low-frequency earthquake swarms, *Nature*, *446*, 305–307.
- Smith, G. P., D. A. Wiens, K. M. Fischer, L. M. Dorman, S. C. Webb, and J. A. Hildebrand (2001), A complex pattern of mantle flow in the Lau back arc, *Science*, *292*, 713–716.
- Stachnik, J. C., G. A. Abers, and D. Christensen (2004), Seismic attenuation and mantle wedge temperatures in the Alaska subduction zone, *J. Geophys. Res.*, *109*, B10304, doi:10.1029/2004JB003018.
- Stein, C. A., and S. Stein (1992), A model for the global variation in oceanic depth and heat flow with lithospheric age, *Nature*, *359*, 123–129.
- Syracuse, E. M., and G. A. Abers (2006), Global compilation of variations in slab depth beneath arc volcanoes and implications, *Geochem. Geophys. Geosyst.*, *7*, Q05017, doi:10.1029/2005GC001045.
- Takahashi, N., S. Kodaira, T. Tsuru, J.-O. Park, Y. Kaneda, K. Suyehiro, H. Kinoshita, S. Abe, M. Nishino, and R. Hino (2004), Seismic structure and seismogenesis off Sanriku region, northeastern Japan, *Geophys. J. Int.*, *159*, 129–145.
- Tatsumi, Y., and S. Eggins (1995), *Subduction Zone Magmatism*, 211 pp., Blackwell Science, Boston.
- Tonarini, S., S. Agostini, C. Doglioni, F. Innocenti, and P. Manetti (2007), Evidence for serpentine fluid in convergent margin systems: The example of El Salvador (Central America) arc lavas, *Geochem. Geophys. Geosyst.*, *8*, Q09014, doi:10.1029/2006GC001508.
- Tono, Y. (2006), Use of Hi-net tiltmeter records to image mantle discontinuities and anisotropic structure beneath the Japanese islands, Ph.D. thesis, 101 pp., Univ. of Tokyo, Japan.
- Tsuji, Y., J. Nakajima, S. Kita, T. Okada, T. Matsuzawa, and A. Hasegawa (2007), Hydrous oceanic crust of the subducting Pacific slab inferred from double difference tomography, paper presented at Symposium 2007 “Dynamic Earth—Its Origin and Future,” Adv. Sci. and Technol. Cent. for the Dynamic Earth, Sendai, Japan.
- Tsumura, N., S. Matsumoto, S. Horiuchi, and A. Hasegawa (2000), Three-dimensional attenuation structure beneath the northeastern Japan arc estimated from spectra of small earthquakes, *Tectonophysics*, *319*, 241–260.
- van Keken, P. E., B. Kiefer, and S. M. Peacock (2002), High-resolution models of subduction zones: Implications for mineral dehydration reactions and the transport of water into the deep mantle, *Geochem. Geophys. Geosyst.*, *3*(10), 1056, doi:10.1029/2001GC000256.
- Wang, K., and J. He (1999), Mechanics of low-stress forearcs: Nankai and Cascadia, *J. Geophys. Res.*, *104*, 15,191–15,205.
- Wang, K., and K. Suyehiro (1999), How does plate coupling affect crustal stresses in Northeast and Southwest Japan?, *Geophys. Res. Lett.*, *26*, 2307–2310.
- Wang, K., T. Mulder, G. C. Rogers, and R. D. Hyndman (1995), Case for very low coupling stress on the Cascadia subduction fault, *J. Geophys. Res.*, *100*, 12,907–12,918.
- Wiens, D. A., and G. P. Smith (2003), Seismological constraints on structure and flow patterns within the mantle wedge, in *Inside the Subduction Factory*, *Geophys. Monogr. Ser.*, vol. 138, edited by J. Eiler, pp. 59–81, AGU, Washington D. C.
- Zhao, D., A. Hasegawa, and S. Horiuchi (1992), Tomographic imaging of P and S wave velocity structure beneath northeastern Japan, *J. Geophys. Res.*, *97*, 19,909–19,928.

J. He, R. D. Hyndman, I. Wada, and K. Wang, Pacific Geoscience Centre, Geological Survey of Canada, 9860 West Saanich Road, P.O. Box 6000, Sidney, BC, Canada V8L 4B2. (ikukow@uvic.ca)